

Removal of Methyl Orange from Aqueous Solutions by Ferromagnetic Fe/Ni Nanoparticles

H. Sarvari^a, E.K. Goharshadi^{a,b,*}, S. Samiee^a and N. Ashraf^a

^aDept. of Chemistry, Ferdowsi University of Mashhad, Mashhad 9177948974, Iran

^bCenter of Nano Research, Ferdowsi University of Mashhad, Mashhad 9177948974, Iran

(Received 4 December 2017, Accepted 20 April 2018)

Herein, the removal of methyl orange (MO), a monoazo dye, from aqueous solutions was investigated using bimetallic ferromagnetic Fe/Ni nanoparticles (NPs) with the average particle size of 12-16 nm. The effect of contact time, pH, temperature, and Fe/Ni dosage on dye removal process was investigated. The results showed that 60 mg of Fe/Ni NPs at 25 °C and pH = 1 can remove 99.5% of 50 mg l⁻¹ dye solution within 15 min. The MO removal follows the pseudo-second-order kinetics with the rate constant of 0.4114 g mg⁻¹ min⁻¹. The chromophore structure of the dye was broken down in the presence of Fe/Ni NPs. The Fe/Ni NPs were prepared by simple co-reduction method and characterized by several techniques including X-ray diffraction, scanning electron microscopy, transmission electron microscopy (TEM), high-resolution TEM, scanning tunneling microscopy, and vibrating sample magnetometer.

Keywords: Ferromagnetic Fe/Ni nanoparticles, Dye removal, Kinetic study, Methyl orange

INTRODUCTION

The release of dye effluents from different industries has turned into a severe environmental problem because of their toxicity, high chemical oxygen demand, *etc.* [1,2] Different techniques have been employed for removal of dyes from aqueous solutions [3,4]. Each technique has some advantages as well as some disadvantages. For example, adsorption is one of the most efficient and promising methods in wastewater treatment because of its simplicity, economically practical, technically feasible, and potential of recycling of the adsorbents. In spite of the advantages, the pollutants are just transferred from one phase to another without any degradation [5,6,7]. In practical applications, almost a combination of two or three methods is necessary to attain the desired result [8,9].

Zero-valent iron, ZVI (Fe⁰) is a cheap and mild reducing agent with an $E^\circ = -0.44$ V. Fe⁰ was used for dye removal from aqueous solutions because of its low-cost, easy

availability, and effectiveness. In addition, it could usually degrade contaminants completely [10]. By reducing the size of iron into the nanoscale, the efficiency of dye degradation increases due to the small particle size and large surface area [11]. Chatterjee *et al.* [12] used micro sized ZVI for the reductive degradation of Reactive Black 5 (RB5) in an aqueous solution. They found that the dye removal efficiency increases with decreasing the initial pH of dye solution. Epolito *et al.* [13] investigated the effect of operational conditions and initial dye concentration on the decolorization of the textile dye Reactive Blue 4 using iron nanoparticles (NPs). They showed that the decolorization rate increases with decreasing pH and raising temperature. Chang *et al.* [14] studied the degradation of two different kinds of dyes, Reactive Blue 4 and RB5, by iron NPs in a N₂ bubbling system (Fe⁰/N₂ process) and air bubbling system (Fe⁰/air process). They found that the Fe⁰/air process shows higher decolorization rate compared to the Fe⁰/N₂ process. However, all of the valuable work suffer from the sensitivity of iron towards oxidation which leads to the corrosion of iron especially by increasing pH. Hence,

*Corresponding author. E-mail: gohari@um.ac.ir

the surface is deactivated over time and the porosity of the surface is reduced [15]. To solve this problem, bimetallic NPs have been introduced. Bimetallic NPs have several applications due to their superior optical, electronic, catalytic, and magnetic properties compared with their monometallic counterparts [16,17]. Several structures are possible for bimetallic NPs including core-shell, cluster-in-cluster, and alloy with an intermetallic compound type, and crown-jewel [18]. The structure may change according to the preparation method [19].

The incorporation of a second metal like Pd, Zn, Ni, or Pt to iron may enhance the dye removal efficiency because it postpones the formation of oxide layer on iron surface [20]. Wang *et al.* [21] used Fe/Pd bimetallic NPs to dechlorinate the chlorinated methanes. Shih *et al.* [22] showed that the reduction efficiencies of hexachlorobenzene (HCB) by Fe and Fe/Pd bimetallic NPs with the same amount of weight at 25 °C are about 60% and 70%, respectively. Although the partial dechlorination was achieved by Fe NPs, Fe/Pd NPs could dechlorinate completely HCB. Samiee *et al.* [23] used Fe/Pd NPs with the average particle size of 36.6 nm to degrade RB5 from aqueous solution. They showed that 0.5 g l⁻¹ Fe/Pd nanoparticles could completely decolorize 20 mg l⁻¹ dye solution at 25 °C. Although adding Pd or Pt to iron enhances the dye removal efficiency greatly, the high cost of the precious metals limits their large-scale applications [24]. Iron-nickel (Fe/Ni) bimetallic NPs have several interesting properties including good corrosion stability, extremely low thermal expansion, remarkable magnetic properties, and low cost of nickel [25]. It was shown both theoretically and experimentally that the Fe/Ni alloy is a good catalyst for CO₂ removal [26]. The Fe/Ni NPs were prepared by various physical and chemical methods [27]. Among these methods, the co-reduction route has several advantages such as simplicity, low-cost, and large-scale production [28].

Herein, we report the preparation and characterization of the Fe/Ni NPs and investigation their efficiency for an azo dye, methyl orange (MO), removal from aqueous solutions. MO is one of the well-known acidic/anionic dyes and is basically used in textile, printing, paper, food, pharmaceutical industries, and in research laboratories as a titration indicator [29]. Due to its harmful impact on the

environment and high solubility in water, it is necessary to remove this dye from aqueous systems [30]. The effect of contact time, pH, temperature, and Fe/Ni dosage on dye removal process was investigated. The adsorption isotherms and kinetic studies of removal of azo dye were analyzed.

EXPERIMENTAL

Materials

Nickel(II) chloride hexahydrate (≥98.0%), iron(II) sulfate heptahydrate (99.5%), methyl orange (ACS, Reag. Ph Eur) from Merck, sodium borohydride (≥98.0%) from Sigma Aldrich, and sodium hydroxide (≥97.00) from Fluka Co were purchased. The chemical materials used in this work were of analytical grade and used as received without further purification. Deionized water was used for preparation of all solutions.

PREPARATION OF Fe/Ni NPs

In a typical procedure, 0.024 mol of FeSO₄·H₂O and 0.0042 mol of NiCl₂·6H₂O were dissolved in deionized water. The reaction vessel was circulated by nitrogen gas to prevent the accumulation of H₂ gas generated during the reduction process. After adjusting pH to 6.20-7.00 with NaOH (1.26 M), 0.053 mol of sodium borohydride, NaBH₄, as the reducing agent was added to the solution. By adding NaBH₄, the pH of solution increased to 10. During the reduction reaction, the color of solution changed from brownish-green to black. The solution was stirred for 15 min and then the NPs were separated by a strong magnet. The NPs were washed several times with deionized water, ethanol, and acetone and then dried at 50 °C under vacuum overnight.

CHARACTERIZATION AND INSTRUMENTS

The powder X-ray diffraction (PXRD) pattern of the NPs was used to determine the phase and crystal structure by means of Bruker/D8 Advanced diffractometer with graphite monochromatic Cu K α radiation ($\lambda = 1.541 \text{ \AA}$) in the 2θ range from 20-80° by step of 0.04 degrees.

The surface area, pore volume, and average pore size of

the sample were measured by an ASAP-2010 system from Micromeritics. The sample was degassed to remove moisture and impurities at 200 °C for 10 h under 50 mTorr vacuum.

The scanning electron microscopy (SEM) analysis was obtained by LEO 1450 VP Model. The transmission electron microscopy (TEM) analysis of the sample was performed using a LEO 912 AB instrument. The electron beam accelerating voltage was 120 kV. The high-resolution TEM (HRTEM) image was taken by FEI Tecnai F20 Field emission using an accelerating voltage of 200 kV. The scanning tunneling microscopy (STM) images of the NPs deposited on highly oriented pyrolytic graphite (HOPG) substrate were provided by STM SS1 with Pt/Ir STM tip, 1.7 nA constant current, and 0.23 V voltage.

The vibrating sample magnetometer (VSM) was used for magnetization measurement. The measurement was taken from 0 to ± 8 kOe fields.

The UV-Vis (UV-Vis) absorbance spectrum was recorded using an Agilent photodiode-array Model 8453 equipped with glass of 1 cm path length at room temperature in air within the range 200-750 nm.

Accurate temperature control is a fundamental requirement for the kinetic studies. For this purpose, the water jacket was connected to a circulating cooling water bath (BL 7100, Major Science).

DYE REMOVAL EXPERIMENTS

In each experiment, Fe/Ni NPs (0.01-0.08 g) were mixed with 40 ml dye solution with different dye concentrations (10-50 mg l⁻¹), pH values (1-9), and temperatures (15-45 °C). At each certain time interval, a sample was drawn and centrifuged. Then, the left out concentration in the supernatant solution was measured by a UV-Vis spectrophotometer with reading the absorbance at a wavelength of maximum absorbance, λ_{max} of MO. The λ_{max} values of MO at pH = 1, 7 and 9 are 508, 466 and 468 nm, respectively. Each experiment continued until no significant change in the dye concentration was observed. All experiments were performed in duplicate to guarantee the reproducibility of the results. The average value of the two measurements was reported. To remove photo-degradation interference, all experiments were performed in dark.

RESULTS AND DISCUSSION

Structural Characteristics

The PXRD pattern of the Fe/Ni NPs is shown in Fig. 1a. The amount of Ni and Fe in Fe/Ni can determine the crystalline structure of the alloy. When the Fe content is less than 50 mol%, the diffraction peaks of (111), (200), and (220) crystal planes belonging to face centered cubic (fcc-JCPDS 47-1417) are appeared in the XRD pattern of Fe/Ni alloy [27]. By increasing the Fe content to over 50 mol% only (110) crystal plane related to body centered cubic (bcc-JCPDS 37-0474) is observed. When the Fe content is between 50 and 60 mol%, a mixture of fcc/bcc phases exists [31]. As Fig. 1a shows, there is only one broad peak around $2\theta = 45^\circ$ which corresponds to (110) plane of bcc structure. The noisy XRD pattern may be related to the magnetic nature of Fe/Ni bimetallic NPs which decreases the signal to noise ratio [32]. The similar results was obtained by Zhang *et al.* [33].

The nitrogen adsorption-desorption isotherm at 76 K for Fe/Ni NPs was investigated. The isotherm is apparently IUPAC fourth isotherm type that is a typical of mesoporous materials. The specific surface area and porosity of Fe/Ni NPs are given in Table 1.

The morphology of the surface of NPs was examined via SEM (Fig. 2a), TEM (Fig. 2c, 2d), HRTEM (2e), the selected area electron diffraction (SAED) (Fig. 2f), and STM (Fig. 2g-2i). As Fig. 2a shows, most of the particles are 3D flowerlike nanostructures composed of smooth nanoplates with a thickness of approximately 50 nm.

The TEM images (Fig. 2b, 2c) of Fe/Ni NPs exhibited the average particle diameter of about 12-16 nm. The NPs formed the chain structure due to the magnetic and electronic interactions [34]. Figure 2d presents a HRTEM image. It exhibits a lattice spacing of 2 Å, originating from the (110) reflection. The SAED was used to identify the crystalline phases (Fig. 2e). The SAED pattern confirms the prepared Fe/Ni NPs are semicrystalline. Figures 2f, 2g and 2h represent the STM images of Fe/Ni NPs recorded at room temperature. According to these images, the diameter of the NPs is approximately 10 nm to 23 nm. Also, the STEM image shows that the Fe/Ni NPs have porous structure. Figure 2g shows a STM line scan starting at the point indicated by the line in Fig. 2h.

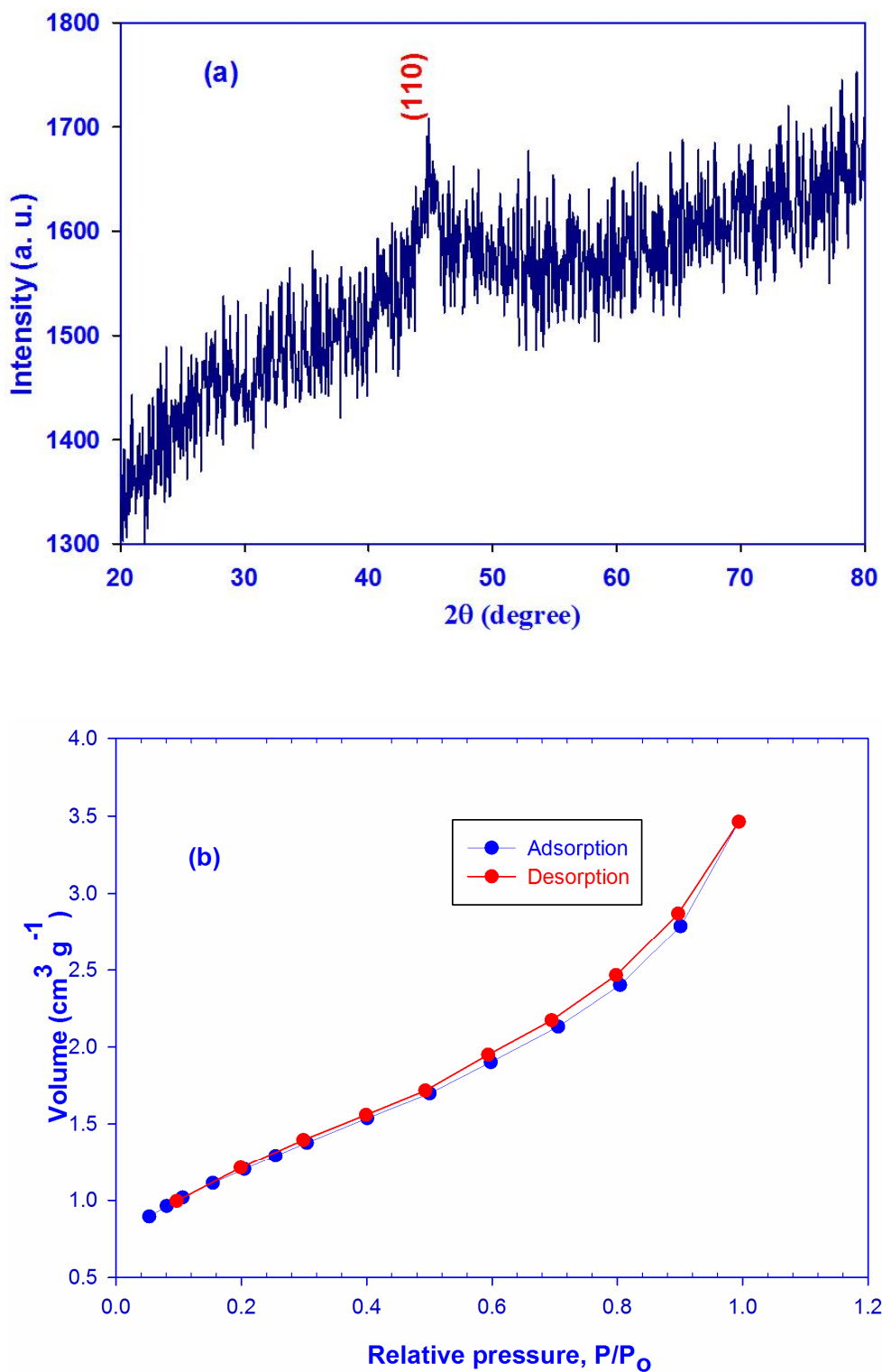


Fig. 1. (a) The XRD pattern, and (b) the nitrogen adsorption-desorption isotherm of Fe/Ni NPs.

Table 1. The Specific Surface Area and Porosity of Fe/Ni NPs

a_{BET}^S (m^2g^{-1}) ^a	a_{BJH}^S (m^2g^{-1}) ^b	V_{BJH}^P (cm^3g^{-1}) ^c	d_{BET} (nm)	d (nm) ^d
34.93	34.75	0.044	8.98	5.000

^aCalculated from BET equation. ^bBJH method adsorption. ^cTotal pore volume for pores with diameters less than 314.93 nm at $p/p_0 = 0.99388$.

^dAverage pore diameter.

Figure 3 displays the magnetic hysteresis (M-H) loop of Fe/Ni NPs at room temperature which indicates they are ferromagnetic. The specific saturation magnetization, M_s , of Fe/Ni NPs is 87 emu g^{-1} which is greater than that of bulk Ni (55 emu g^{-1}) [35] and smaller than that of bulk Fe (220 emu g^{-1}) [36]. Liu *et al.* [37] showed that by increasing the Ni content in Fe/Ni alloy, the M_s value decreases. Hence, in this work, the presence of 20 mol% Ni in the alloy has decreased M_s value in comparison with bulk Fe. This phenomenon can be related to the lattice structure change from bcc to fcc by increasing the Ni content as described in the XRD of the NPs. The coercivity, H_c , and remanence, M_r , of Fe/Ni NPs are 285.7 Oe and 16.67 emu g^{-1} , respectively.

EFFECT OF EXPERIMENTAL PARAMETERS ON DYE REMOVAL PROCESS

The MO removal studies were carried out for different Fe/Ni doses, temperatures, pHs, contact times, and dye concentrations. The dye removal efficiency (DRE%) is defined as:

$$\text{DRE\%} = \frac{q_o - q_t}{q_o} \times 100 \quad (1)$$

where q_o is the amount of MO removed (mg g^{-1}) at initial. q_t (mg g^{-1}) is the amount of MO removed at time t (min) and defined as:

$$q_t = \frac{V(C_o - C_t)}{m} \quad (2)$$

where V is the volume of the solution (l). C_o and C_t (mg l^{-1}) are the dye concentrations initial and time t . m (g) stands for the mass of Fe/Ni NPs.

Dosage of Fe/Ni NPs

The effect of Fe/Ni dosage on MO removal was investigated in the range of 10-80 mg at $\text{pH} = 7$ and $25 \text{ }^\circ\text{C}$. The dye concentration was chosen as 10 mg l^{-1} . Figure 4a shows that as the Fe/Ni dosage increases, the DRE% enhances due to increasing the accessible sites. Of course, the DRE% increases with increasing the Fe/Ni NPs dosage up to 60 mg. Further increasing did not affect the DRE%. Hence, the optimum dosage of Fe/Ni was chosen to be 60 mg for the subsequent experiments.

Temperature

For investigating the effect of temperature, the MO removal by Fe/Ni NPs was carried out at 15, 25, 35 and $45 \text{ }^\circ\text{C}$. By raising temperature from 15 to $25 \text{ }^\circ\text{C}$, the DRE% increased from 94.57% to 97.60%, respectively. It is plausible to say that the MO removal by Fe/Ni NPs may be a kinetically controlled process [38]. After $25 \text{ }^\circ\text{C}$, raising the temperature had no significant effect on the DRE%. Hence, $25 \text{ }^\circ\text{C}$ was chosen as the optimum temperature for removal of MO in the next experiments.

pH

The solution pH is an important parameter in removal of dye molecules. In this work, the pH values of 1, 7 and 9 were chosen. Table 2 represents the results of the effect of the initial pH of the solution on the MO removal efficiency by Fe/Ni NPs for different initial dye concentrations ranging

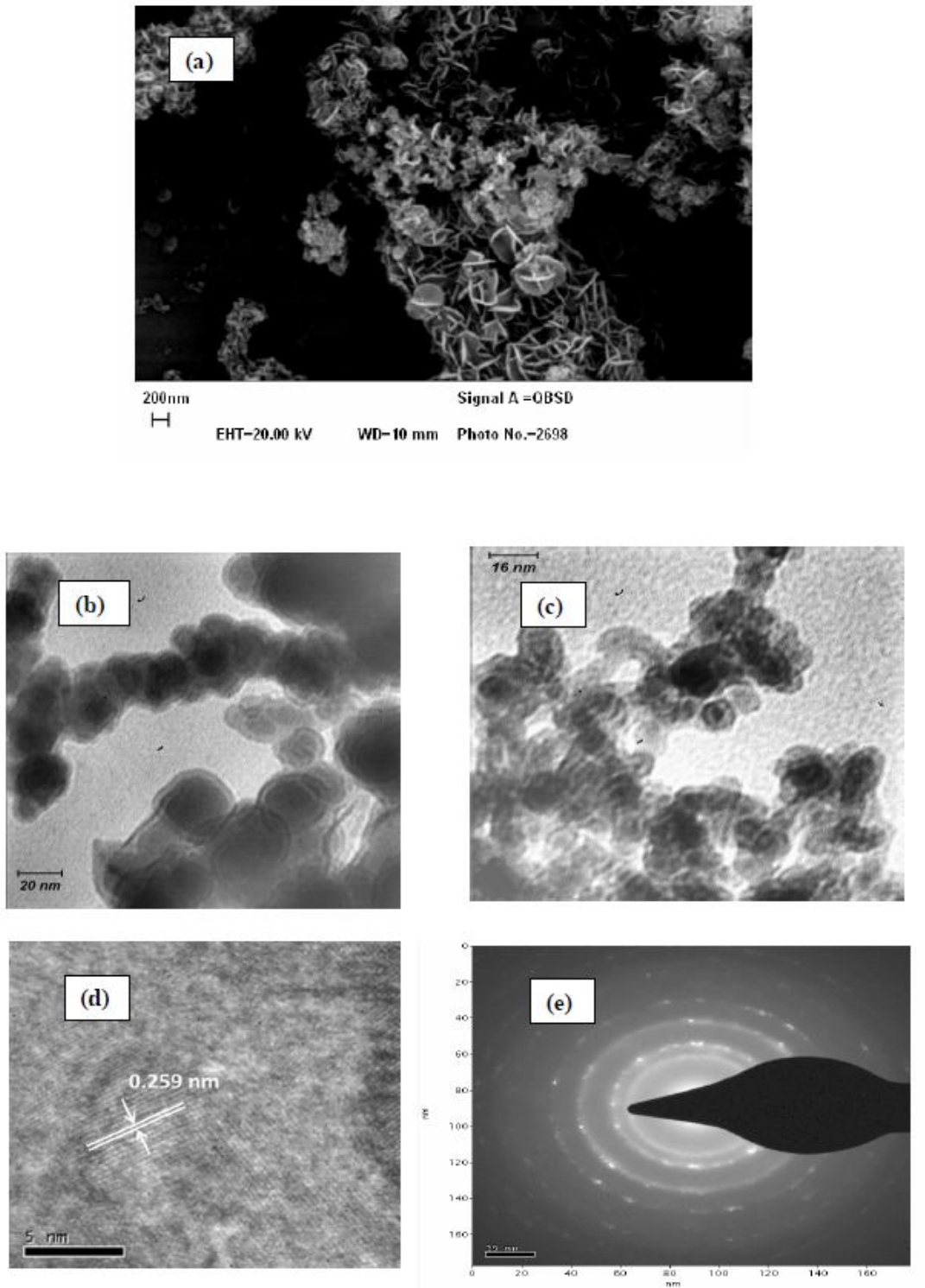


Fig. 2. (a) The SEM image, (b) and (c) TEM images with two magnifications, (d) HRTEM image, (e) SAED, and (f), (g) and (h) STM images of Fe/Ni NPs.

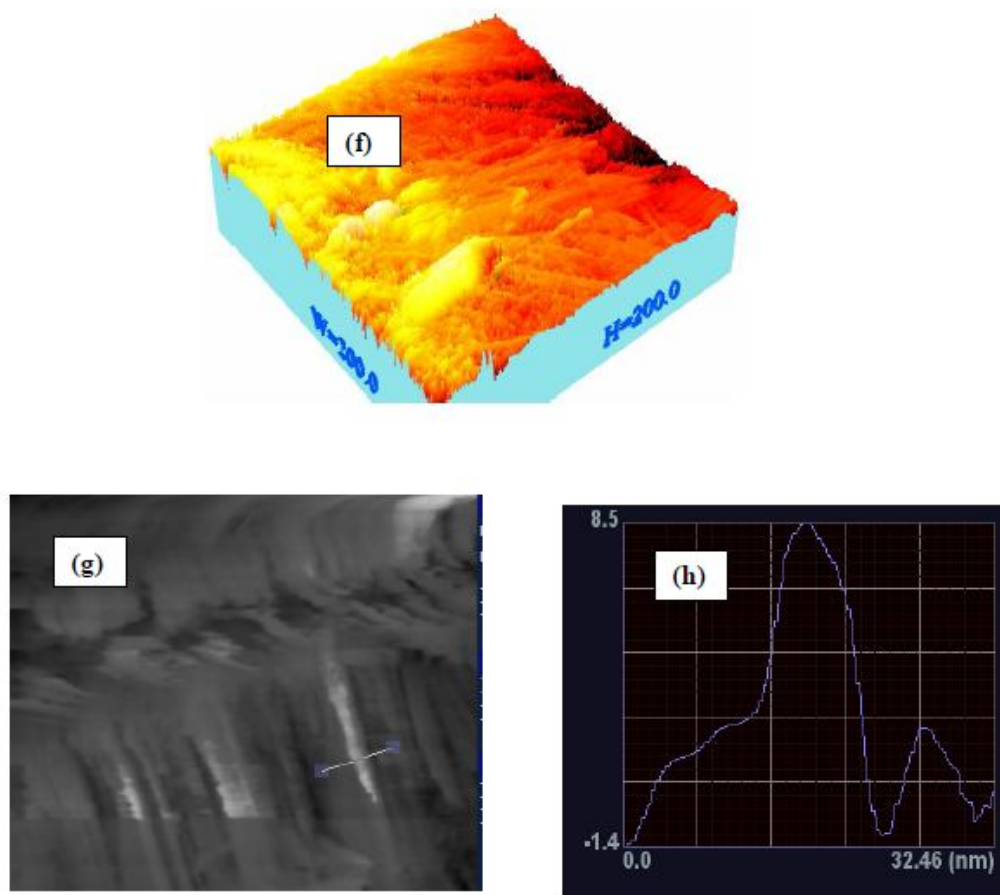


Fig. 2. Continued.

from 10-50 mg l⁻¹. Under alkaline conditions, Fe/Ni NPs are not active due to the formation of a hydroxide layer on the surface of NPs [39]. As Table 2 shows, the removal of MO above 99% was achieved at pH = 1. This pH was selected as the optimum pH for the subsequent experiments.

Dye Concentration

The initial dye concentration is another important variable that can affect the dye removal process [40]. The initial concentration of MO was chosen in the range of 10-50 mg l⁻¹ (Fig. 4b). According to Fig. 4b, MO removal slightly decreases from around 99.5% at a concentration of 50 mg l⁻¹ to 98.5% when the concentration decreased to 10 mg l⁻¹.

Contact Time

The contact time is the most important design parameter that influences the performance of a dye removal. The effect of contact time on the removal of MO by Fe/Ni NPs was illustrated in Fig. 4c. The solution pH and Fe/Ni dosage were fixed at 1 and 60 mg, respectively. This figure shows that the dye removal is very fast.

KINETIC STUDIES

The kinetics of MO removal by Fe/Ni NPs was studied using UV-Vis spectroscopy. Figure 5 shows that MO could be removed completely by Fe/Ni NPs in an aqueous solution after 8 min. The intensity of the absorption peak at

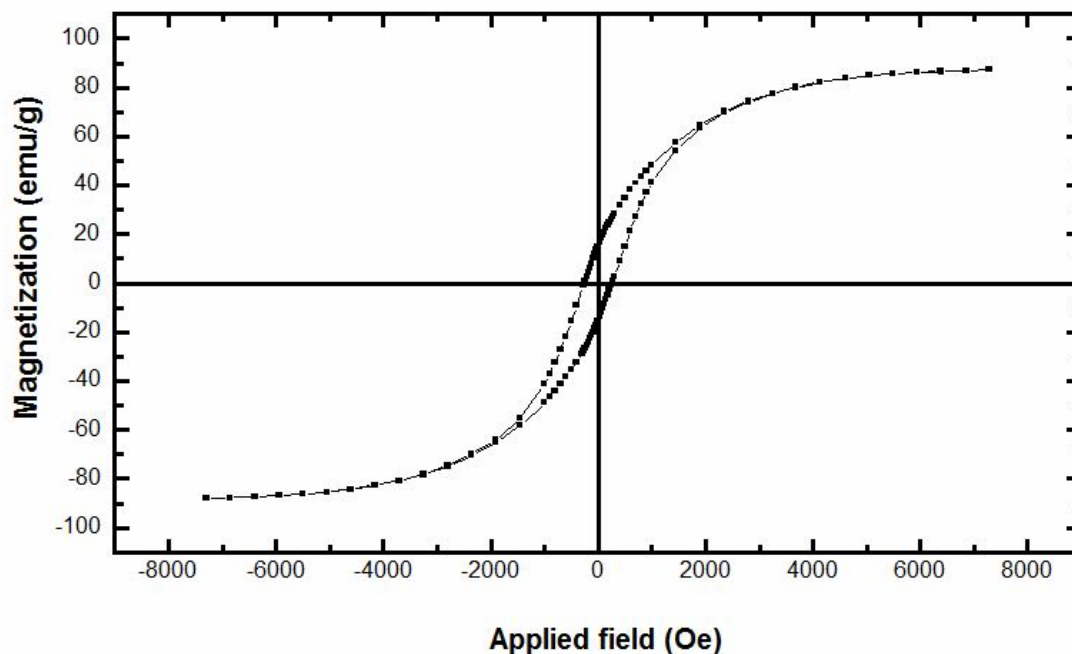


Fig. 3. The magnetic hysteresis loops of Fe/Ni NPs.

Table 2. The Effect of pH on DRE% for 60 mg Fe/Ni NPs at 25 °C

Initial dye concentration (mg l ⁻¹)	pH = 1		pH = 7		pH = 9	
	Time	DRE	Time	DRE	Time	DRE
	(min)	(%)	(min)	(%)	(min)	(%)
10	9	98.50	5	97.24	25	97
20	11	99.12	12	95.00		
30	11	99.40	12	97.00		
40	14	99.50	9	97.00		
50	15	99.50	12	97.60		

508 nm diminishes to zero. It shows that the chromophore structure of the dye was broken down in the presence of Fe/Ni NPs [41].

The kinetic of MO removal by Fe/Ni NPs was investigated using the common kinetic models. The pseudo-

first order equation is expressed as [42]:

$$\frac{dq_t}{dt} = k_1(q_e - q_t) \quad (3)$$

where k_1 is the rate constant (min⁻¹). q_e is the value of

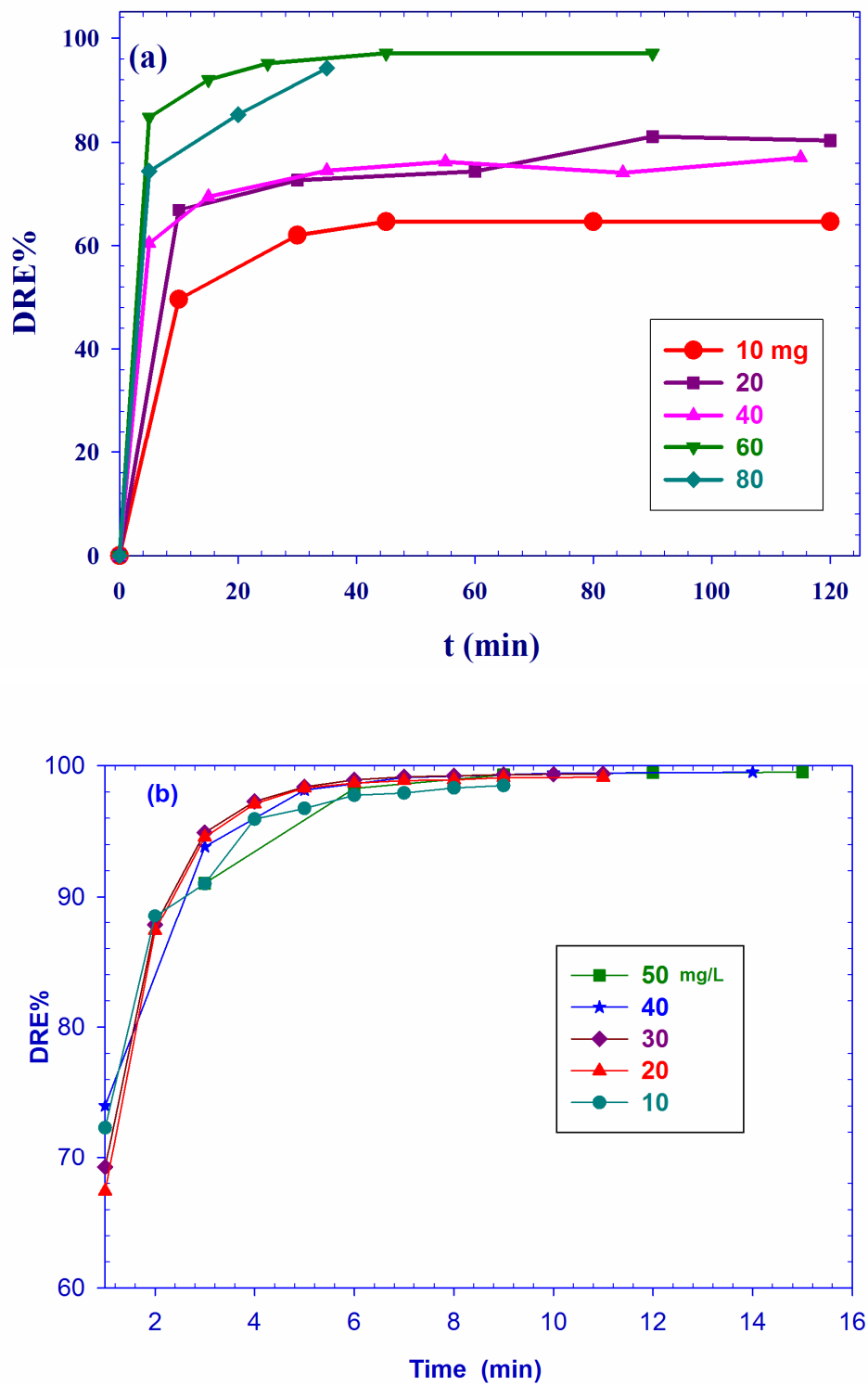


Fig. 4. The effect of (a) Fe/Ni NPs dosage, (b) dye concentration, and (c) adsorption capacity versus time at different initial dye concentrations.

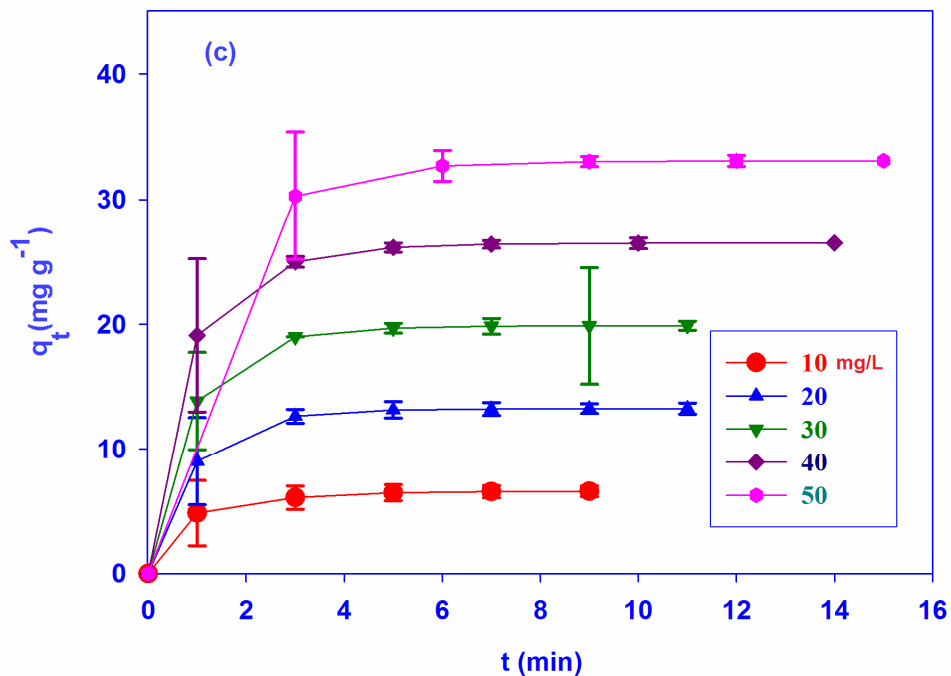


Fig. 4. Continued.

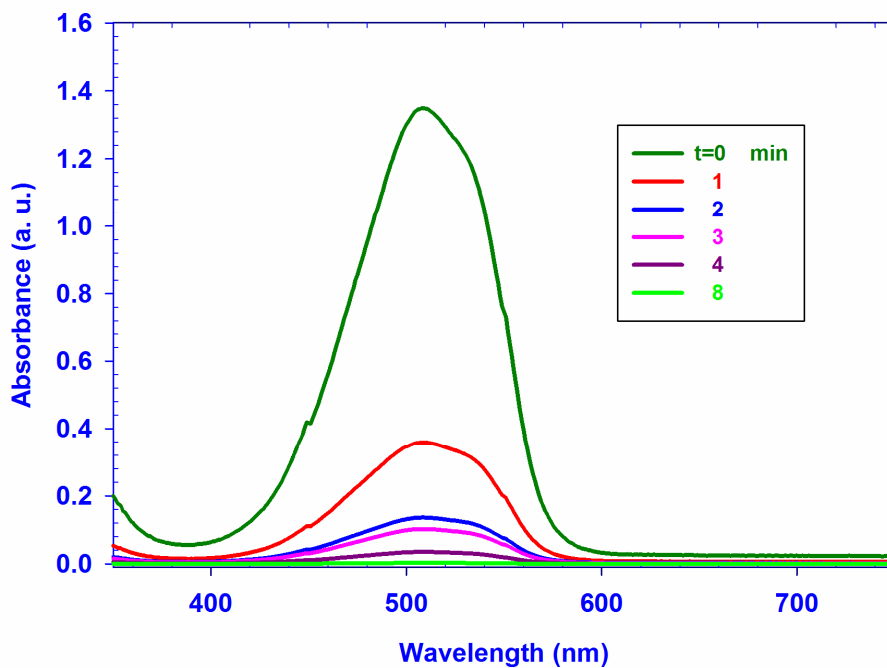
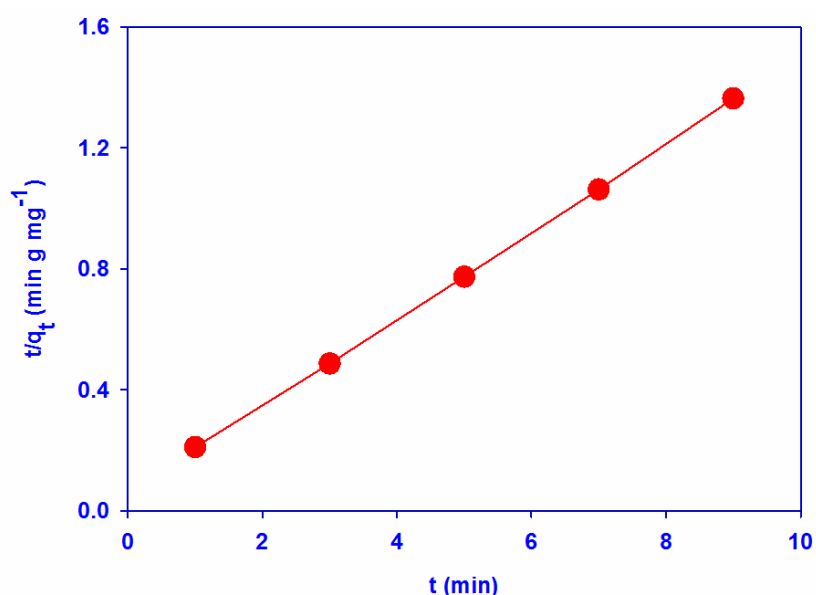


Fig. 5. The variation in UV-Vis spectrum of Mo during the dye removal process by Fe/Ni NPs (25 °C, Fe/Ni NPs dosage = 60 mg, concentration of MO dye solution = 50 mg l⁻¹, initial pH = 1).

Table 3. The Rate Constants and the Calculated and Experimental q_e Values for MO Removal by Fe/Ni NPs

First-order kinetic model					Second-order kinetic model			
q_e (exp)	k_1 (mg g^{-1})	q_e (cal)	R^2 (min^{-1})	se (mg g^{-1})	k_2 ($\text{g mg}^{-1} \text{min}^{-1}$)	q_e (cal)	R^2	se
6.66	0.6888	3.00	0.9934	0.114	0.4114	6.88	0.9997	0.005

**Fig. 6.** Pseudo-second-order kinetic model for Mo removal by Fe/Ni NPs (25 °C, pH = 1, 60 mg Fe/Ni, 10 mg l⁻¹ dye).

equilibrium adsorption capacity (mg g^{-1}).

The integrated form of Eq. (2) is:

$$\ln(q_e - q_t) = \ln q_e - k_1 t \quad (4)$$

The pseudo-second order equation can be represented as:

43

$$\frac{dq_t}{dt} = k_2 (q_e - q_t)^2 \quad (5)$$

where k_2 is the rate constant ($\text{g mg}^{-1} \text{min}^{-1}$). The integrated form is:

Both Fig. 6 and Table 3 show that the MO removal by Fe/Ni NPs follows the pseudo-second-order. Table 3 shows that the experimental value of q_e is very close to that of calculated by the pseudo-second-order. The correlation coefficients (Table 3) show that pseudo-second-order model is more appropriate.

CONCLUSIONS

This study demonstrates the ability of Fe/Ni NPs for removal an azo dye from aqueous solution. The MO removal was very fast and followed the pseudo-second-

order kinetic model. The ferromagnetic Fe/Ni nanoparticles (NPs) with the average particle size of 12-16 nm, BET surface area of $34.93 \text{ m}^2 \text{ g}^{-1}$, and specific saturation magnetization of 87 emu g^{-1} were prepared. The experimental results showed that the solution pH, Fe/Ni dosage, and the initial dye concentration are the main effective factors on MO removal using Fe/Ni NPs. The results showed that 0.06 g of Fe/Ni NPs at 25 °C and pH = 1 can remove 99.5% of 50 mg l⁻¹ dye solution within 15 min.

ACKNOWLEDGEMENTS

The authors express their gratitude to Ferdowsi University of Mashhad in support of this project (P736).

REFERENCES

- [1] Siddique, M.; Farooq, R.; Khalid, A.; Farooq, A.; Mahmood, Q.; Farooq, U.; Raja, I. A.; Shaukat, S. F., Thermal-pressure-mediated hydrolysis of Reactive Blue 19 dye. *J. Hazard. Mater.* **2009**, *172*, 1007-1012. DOI: <https://doi.org/10.1016/j.jhazmat.2009.07.095>.
- [2] Samiee, S.; Goharshadi, E. K., Graphene nanosheets as efficient adsorbent for an azo dye removal: kinetic and thermodynamic studies. *J. Nanopart. Res.* **2014**, *16*, 2542. DOI: <https://doi.org/10.1007/s11051-014-2542-8>.
- [3] Lin, S. H.; Peng, C. F., Continuous treatment of textile wastewater by combined coagulation, electrochemical oxidation and activated sludge. *Water Res.* **1996**, *30*, 587-592. DOI: [https://doi.org/10.1016/0043-1354\(95\)00210-3](https://doi.org/10.1016/0043-1354(95)00210-3).
- [4] Tanaka, K.; Padermpole, K.; Hisanaga, T., Photocatalytic degradation of commercial azo dyes. *Water Res.* **2000**, *34*, 327-333. DOI: [https://doi.org/10.1016/S0043-1354\(99\)00093-7](https://doi.org/10.1016/S0043-1354(99)00093-7).
- [5] Yazdanbakhsh, M.; Khosravi, I.; Goharshadi, E. K.; Youssefi, A., Fabrication of nanospinel ZnCr₂O₄ using sol-gel method and its application on removal of azo dye from aqueous solution. *J. Hazard. Mater.* **2010**, *184*, 684-689. DOI: <https://doi.org/10.1016/j.jhazmat.2010.08.092>.
- [6] Khosravi, I.; Yazdanbakhsh, M.; Goharshadi, E. K.; Youssefi, A., Preparation of nanospinels NiMn_xFe_{2-x}O₄ using sol-gel method and their applications on removal of azo dye from aqueous solutions. *Mate. Chem. Phys.* **2011**, *130*, 1156-1161. DOI: <https://doi.org/10.1016/j.matchemphys.2011.08.048>.
- [7] Goharshadi, E. K.; Hadadian, M.; Karimi, M.; Azizi-Toupkanloo, H., Photocatalytic degradation of reactive black 5 azo dye by zinc sulfide quantum dots prepared by a sonochemical method. *Mater. Sci. Semicond. Process.* **2013**, *16*, 1109-1116. DOI: <https://doi.org/10.1016/j.mssp.2013.03.005>.
- [8] Mahvelati-Shamsabadi, T.; Goharshadi, E., Photostability and visible-light-driven photoactivity enhancement of hierarchical ZnS nanoparticles: The role of embedment of stable defect sites on the catalyst surface with the assistant of ultrasonic waves. *Ultrason. Sonochem.* **2017**, *34*, 78-89. DOI: [10.1016/j.ultsonch.2016.05.021](https://doi.org/10.1016/j.ultsonch.2016.05.021).
- [9] Karimi-Nazarabad, M.; Goharshadi, E. K., Highly efficient photocatalytic and photoelectrocatalytic activity of solar light driven WO₃/g-C₃N₄ nanocomposite. *Sol. Energy Mater. Sol. Cells* **2017**, *160*, 484-493. DOI: [10.1016/j.solmat.2016.11.005](https://doi.org/10.1016/j.solmat.2016.11.005).
- [10] Johnson, T. L.; Scherer, M. M.; Tratnyek, P. G., Kinetics of halogenated organic compound degradation by iron metal. *Environ. Sci. & Technol.* **1996**, *30*, 2634-2640. DOI: [10.1021/es9600901](https://doi.org/10.1021/es9600901).
- [11] Moon, B. H.; Park, Y. B.; Kim, S. S.; Seo, G. T.; Lee, T. S.; Kim, T. S., *Mater. Sci. Forum* **2007**, *544-545*, 705-708.
- [12] Chatterjee, S.; Lim, S. -R.; Woo, S. H., Removal of Reactive Black 5 by zero-valent iron modified with various surfactants. *Chem. Eng. J.* **2010**, *160*, 27-32. DOI: <https://doi.org/10.1016/j.cej.2010.02.045>.
- [13] Epolito, W. J.; Yang, H.; Bottomley, L. A.; Pavlostathis, S. G., Kinetics of zero-valent iron reductive transformation of the anthraquinone dye Reactive Blue 4. *J. Hazard. Mater.* **2008**, *160*, 594-600. DOI: <https://doi.org/10.1016/j.jhazmat.2008.03.033>.
- [14] Chang, S. -H.; Wang, K. -S.; Chao, S. -J.; Peng, T. -H.; Huang, L. -C., Degradation of azo and anthraquinone dyes by a low-cost Fe⁰/air process. *J.*

- Hazard. Mater.* **2009**, *166*, 1127-1133. DOI: <https://doi.org/10.1016/j.jhazmat.2008.12.021>.
- [15] Liu, Y.; Majetich, S. A.; Tilton, R. D.; Sholl, D. S.; Lowry, G. V., TCE dechlorination rates, pathways, and efficiency of nanoscale iron particles with different properties. *Environ. Sci. Technol.* **2005**, *39*, 1338-1345. DOI: 10.1021/es049195r
- [16] Wang, D.; Li, Y., Bimetallic nanocrystals: liquid-phase synthesis and catalytic applications. *Adv. Mater.* **2011**, *23*, 1044-1060. DOI: 10.1002/adma.201003695.
- [17] Azizi-Toupanloo, H.; Goharshadi, E. K.; Nancarrow, P., Structural, electrical and rheological properties of palladium/silver bimetallic nanoparticles prepared by conventional and ultrasonic-assisted reduction methods. *Adv. Powder Technol.* **2014**, *25*, 801-810. DOI: <https://doi.org/10.1016/j.apt.2013.11.015>.
- [18] Hwang, B. -J.; Sarma, L. S.; Chen, J. -M.; Chen, C. -H.; Shih, S. -C.; Wang, G. -R.; Liu, D. -G.; Lee, J. -F.; Tang, M. -T., Structural models and atomic distribution of bimetallic nanoparticles as investigated by X-ray absorption spectroscopy. *J. Am. Chem. Soc.* **2005**, *127*, 11140-11145. DOI: 10.1021/ja0526618.
- [19] Annadurai, G.; Ling, L. Y.; Lee, J. -F., Adsorption of reactive dye from an aqueous solution by chitosan: isotherm, kinetic and thermodynamic analysis. *J. Hazard. Mater.* **2008**, *152*, 337-346. DOI: <https://doi.org/10.1016/j.jhazmat.2007.07.002>.
- [20] Feng, J.; Lim, T. -T., Pathways and kinetics of carbon tetrachloride and chloroform reductions by nano-scale Fe and Fe/Ni particles: comparison with commercial micro-scale Fe and Zn. *Chemosphere* **2005**, *59*, 1267-1277. DOI: <https://doi.org/10.1016/j.chemosphere.2004.11.038>.
- [21] Wang, X.; Chen, C.; Chang, Y.; Liu, H., Dechlorination of chlorinated methanes by Pd/Fe bimetallic nanoparticles. *J. Hazard. Mater.* **2009**, *161*, 815-823. DOI: <https://doi.org/10.1016/j.jhazmat.2008.04.027>.
- [22] Shih, Y. -h.; Chen, Y. -C.; Chen, M. -Y.; Tai, Y. -T.; Tso, C. -P., Dechlorination of hexachlorobenzene by using nanoscale Fe and nanoscale Pd/Fe bimetallic particles. *Colloids Surf. A: Physicochemical and Engineering Aspects* **2009**, *332*, 84-89. DOI: <https://doi.org/10.1016/j.colsurfa.2008.09.031>.
- [23] Samiee, S.; Goharshadi, E. K.; Nancarrow, P., Successful degradation of Reactive Black 5 by engineered Fe/Pd nanoparticles: Mechanism and kinetics aspects. *J. Taiwan Institute .Chem. Eng.* **2016**, *67*, 406-417. DOI: <https://doi.org/10.1016/j.jtice.2016.07.012>.
- [24] Xu, J.; Bhattacharyya, D., Modeling of Fe/Pd nanoparticle-based functionalized membrane reactor for PCB dechlorination at room temperature. *J. Phys. Chem. C* **2008**, *112*, 9133-9144. DOI: 10.1021/jp7097262.
- [25] Folch, B.; Larionova, J.; Guari, Y.; Datas, L.; Guerin, C., A coordination polymer precursor approach to the synthesis of NiFe bimetallic nanoparticles within hybrid mesoporous silica. *J. Mater. Chem.* **2006**, *16*, 4435-4442. DOI: 10.1039/B608058H.
- [26] Cheng, D.; Negreiros, F. R.; Apra, E.; Fortunelli, A., Computational approaches to the chemical conversion of carbon dioxide. *Chem. Sus. Chem.* **2013**, *6*, 944-965. DOI: 10.1002/cssc.201200872.
- [27] Xiang, J.; Shen, X.; Song, F.; Liu, M.; Zhou, G.; Chu, Y., Fabrication and characterization of Fe-Ni alloy/nickel ferrite composite nanofibers by electrospinning and partial reduction. *Mater. Res. Bull.* **2011**, *46*, 258-261. DOI: <https://doi.org/10.1016/j.materresbull.2010.11.004>.
- [28] Liu, L.; Guan, J.; Shi, W.; Sun, Z.; Zhao, J., Facile synthesis and growth mechanism of flowerlike Ni-Fe alloy nanostructures. *J. Phys. Chem. C* **2010**, *114*, 13565-13570. DOI: 10.1021/jp104212v.
- [29] Haque, E.; Lee, J. E.; Jang, I. T.; Hwang, Y. K.; Chang, J. -S.; Jegal, J.; Jhung, S. H., Adsorptive removal of methyl orange from aqueous solution with metal-organic frameworks, porous chromium-benzenedicarboxylates. *J. Hazard. Mater.* **2010**, *181*, 535-542. DOI: <https://doi.org/10.1016/j.jhazmat.2010.05.047>.
- [30] Chen, S.; Zhang, J.; Zhang, C.; Yue, Q.; Li, Y.; Li, C., Equilibrium and kinetic studies of methyl orange and methyl violet adsorption on activated carbon

- derived from *Phragmites australis*. *Desalination* **2010**, 252, 149-156. DOI: <https://doi.org/10.1016/j.desal.2009.10.010>.
- [31] Leith, S. D.; Ramli, S.; Schwartz, D. T., Characterization of Ni_xFe_{1-x} (0.10 < x < 0.95) electrodeposition from a family of sulfamate-chloride electrolytes. *J. Electrochem. Soc.* **1999**, 146, 1431-1435. DOI: 10.1149/1.1391781.
- [32] Suryanarayana, C.; Norton, M. G., X-Ray Diffraction: A Practical Approach. Springer Science & Business Media, 1998.
- [33] Zhang, W.; Quan, X.; Wang, J.; Zhang, Z.; Chen, S., Rapid and complete dechlorination of PCP in aqueous solution using Ni-Fe nanoparticles under assistance of ultrasound. *Chemosphere* **2006**, 65, 58-64. DOI: <https://doi.org/10.1016/j.chemosphere.2006.02.060>.
- [34] Zhang, L.; Manthiram, A., Chains composed of nanosize metal particles and identifying the factors driving their formation. *Appl. Phys. Lett.* **1997**, 70, 2469-2471. DOI: <https://doi.org/10.1063/1.118859>.
- [35] Jia, F. L.; Zhang, L. Z.; Shang, X. Y.; Yang, Y., Non-aqueous sol-gel approach towards the controllable synthesis of nickel nanospheres, nanowires, and nanoflowers. *Adv. Mater.* **2008**, 20, 1050-1054. DOI: 10.1002/adma.200702159.
- [36] Ogawa, T.; Seto, K.; Hasegawa, D.; Yang, H.; Kura, H.; Takahashi, M., Effect of nucleation and growth dynamics on saturation magnetization of chemically synthesized Fe nanoparticles. *J. Magn.* **2011**, 16, 308-311. DOI: 10.4283/JMAG.2011.16.3.308.
- [37] Liu, Y.; Chi, Y.; Shan, S.; Yin, J.; Luo, J.; Zhong, C.-J., Characterization of magnetic NiFe nanoparticles with controlled bimetallic composition. *J. Alloys Compd.* **2014**, 587, 260-266. DOI: <https://doi.org/10.1016/j.jallcom.2013.10.203>.
- [38] Doğan, M.; Özdemir, Y.; Alkan, M., Adsorption kinetics and mechanism of cationic methyl violet and methylene blue dyes onto sepiolite. *Dyes and Pigments* **2007**, 75, 701-713. DOI: <https://doi.org/10.1016/j.dyepig.2006.07.023>.
- [39] Zhang, H.; Duan, L.; Zhang, Y.; Wu, F., The use of ultrasound to enhance the decolorization of the C.I. Acid Orange 7 by zero-valent iron. *Dyes Pigments* **2005**, 65, 39-43. DOI: 10.1016/j.dyepig.2004.06.015
- [40] Moussavi, G.; Mahmoudi, M., Removal of azo and anthraquinone reactive dyes from industrial wastewaters using MgO nanoparticles. *J. Hazard. Mater.* **2009**, 168, 806-812. DOI: <https://doi.org/10.1016/j.jhazmat.2009.02.097>.
- [41] Oakes, J.; Gratton, P., Kinetic investigations of the oxidation of Methyl Orange and substituted arylazonaphthol dyes by peracids in aqueous solution. *J. Chem. Soc. Perkin Transactions 2* **1998**, 2563-2568. DOI: 10.1039/a807272h
- [42] Lagergren, S., Kungliga Svenska Vetenskapsakademien Handlingar. *Band.* **1898**, 24, 1-39.
- [43] Ho, Y. -S.; McKay, G., Pseudo-second order model for sorption processes. *Process Biochem.* **1999**, 34, 451-465. DOI: [https://doi.org/10.1016/S0032-9592\(98\)00112-5](https://doi.org/10.1016/S0032-9592(98)00112-5).